Sodium and acidic alginate foams with hierarchical porosity: Preparation, characterization and efficiency as a dye adsorbent

Asja Pettignano, Nathalie Tanchoux, Thomas Cacciaguerra, Thierry Vincent, Luca Bernardi, Eric Guibal, Francoise Quignard

Sodium and acidic alginate foams with hierarchical porosity: preparation, characterization and efficiency as a dye adsorbent

Asja Pettignano [a,b], Nathalie Tanchoux [a], Thomas Cacciaguerra[a], Thierry Vincent [c], Luca Bernardi [b*], Eric Guibal [c], Françoise Quignard [a]*

[a] Institut Charles Gerhardt, CNRS-ENSCM-UM, 8 Rue Ecole Normale, 34296, Montpellier-France

[b] Department of Industrial Chemistry "Toso Montanari", University of Bologna, V. Risorgimento, 4, 40136, Bologna. Italy

[c] Ecole des Mines d'Alès, C2MA/MPA, 6 Avenue de Clavières, 30319, Alès. France

ABSTRACT: A novel approach for the preparation of sodium alginate foams by ice-templating, followed by freeze-drying was described. Important effects of the preparation parameters on the macroporous structure of the final materials could be evidenced. A functionalization procedure for the preparation of acidified macro/meso-porous foams with high surface area was optimized and the efficiency of one alginic acid foam was demonstrated for the adsorption of a basic dye (methylene blue) from aqueous solution. The comparison of the maximum monolayer adsorption capacity of this adsorbent with the values already reported for other biosorbents clearly identified

alginic acid foams as competitive sorbents for the removal of methylene blue from aqueous solutions.

KEYWORDS: foams, hierarchical porosity, biopolymers, alginic acid, biocompatible adsorbent, CT-scan.

1. INTRODUCTION

Alginate-based materials have been extensively studied for the sorption of metal ions (An, Lee, Lee, Lee, & Choi, 2015), the encapsulation of bioactive molecules (Hadinoto & Yang, 2014; Raei, Rajabzadeh, Zibaei, Jafari, & Sani, 2015; Sarker et al., 2015) and the immobilization of organic or inorganic exchangers (Guibal, Vincent, & Jouannin, 2009; Krys et al., 2013; Jung et al., 2015; Vincent et al., 2015; Pandey, & Ramontja, 2016; Pandey, 2017). The presence of carboxylic groups may explain these different applications, thanks to the ability of carboxylic ions (present on mannuronic (M) and guluronic (G) acid moieties) to bind metal ions and to form gels by ionotropic gelation (Agulhon, Markova, Robitzer, Quignard, & Mineva, 2012; Agulhon, Robitzer, David, & Quignard, 2012). Though most of the applications dealing with alginate gels use bead shaping, obtained by the gelling of sodium alginate drops into a calcium chloride solution, several studies have recently investigated the possibility of elaborating foams and sponges (Shapiro, & Cohen, 1997; Ki, Singh, Kim, Son, & Han, 2013). The concept of the elaboration of these alginate foams is based on the ionotropic gelation of the biopolymer solution in a mold, followed by freezing and final freeze-drying. These recent studies are opening a number of new modes of application of these materials allowing, for example, the development of macro-porous “reactive-filtration” systems for environmental applications (sorption), antimicrobial supports, supported catalysis, biomedical devices, etc (Shapiro, & Cohen, 1997; Zmora, Glicklis, & Cohen, 2002;

Jouannin et al., 2011). In this paper, we describe the synthesis of novel sodium alginate foams through the ice-templating technique, followed by freeze-drying, without a gelation step. The ice-templating technique, which uses the directional growth of ices crystals as a template, has been successfully used to synthesize ordered inorganic materials (Klotz, Amirouche, Guizard, Viazzi, & Deville 2012; Dhainaut, Deville, Amirouche, & Klotz, 2016). A special attention was devoted to the process parameters such as the concentration of the biopolymer, the characteristics of the biopolymer (molecular weight, M/G ratio), and the freezing temperature. Sodium alginate foams were finally acidified to obtain water insoluble alginic acid foams with a high concentration of acidic groups and a satisfactory surface area.

In recent times, water pollution due to organic dyes has become a serious environmental problem (Pandey, & Ramontja, 2016; Pandey, 2017). The development of low-cost adsorbents is an extremely attractive strategy for wastewater remediation and natural biopolymers are often presented as abundant, renewable and biodegradable replacements for conventional adsorbents (Rafatullaha, Sulaimana, Hashima, & Ahmadb, 2010; Crini, 2005). Since the carboxylic functional groups contained in the alginic acid structure may allow the formation of acid-base interactions (See Supplementary Material Figure S1), a first example of application is the use of alginic acid foams for the sorption of a basic dye, methylene blue (3,7-bis(dimethylamino)phenothiazin-5-ium chloride trihydrate, MB).

2. EXPERIMENTAL SECTION

2.1. Materials

Two different sodium alginate samples provided by FMC (Protanal LF 240D and LF 200S) were used as received for the preparation of the foams. The respective M/G (mannuronate/ guluronate) ratio of Protanal samples were determined by ^{1}H NMR spectrometry, showing that Protanal LF

200S (**AG1**) contained a higher amount of guluronate groups (M/G: 0.59 i.e. 63% G) whereas Protanal LF 240D (**AG2**) was richer in mannuronate groups (M/G: 2.03 i.e. 33% G). The molecular weights of the two samples of alginate were determined by viscosimetry following a procedure previously published elsewhere (Martinsen, Skjakbraek, Smidsrod, Zanetti, & Paoletti, 1991): Mw = 155000 $g.mol^{-1}$ for **AG1** (viscosity in a 1% solution: 306 Cp, given by the provider) and Mw = 95000 $g.mol^{-1}$ for **AG2** (viscosity in a 1% solution: 115 Cp given by the provider). The viscosities of the aqueous solutions containing different amounts of alginate were performed using a Visco Star Plus viscosimeter as described in a previous study (Pettignano, 2016). Methylene Blue (MB) was purchased from Sigma Aldrich and the dye content of the relative batch was of 96%. Analytical grade solvents and commercially available reagents were used as received.

2.2. Preparation of sodium alginate macroporous foams

Stock solution of sodium alginate were prepared by dissolving the appropriate amount of sodium alginate powder in demineralized Milli-Q water, followed by mechanical agitation in a homogeneous mixer at room temperature for 2 h, so as to obtain a homogeneous solution. The next step consisted in the distribution of the viscous mixture in moulds (plates formed of cylindrical holes of 5 to 8.5 cm diameter and 0.5 cm depth) that were maintained overnight at either -20°C or -80 °C as freezing temperature or 30 min in liquid nitrogen. Finally, the obtained materials were freeze-dried (Alpha 1–4 LD freeze-dryer - Christ, Sigma) at -54°C. 12 different samples were synthesized for each experimental condition used. All 12 samples were, for each experiment, very similar, and were used indifferently for the characterization procedures or adsorption experiments.

2.3. Preparation of alginic acid macro-mesoporous foams

The resulting sodium alginate foams were functionalized by immersion into a distilled water bath, suitably acidified by means of 1M HCl (4x stoichiometric amount), for a minimum exchange

time of 16 h under slow stirring. The so-obtained materials were either dried under supercritical CO_2 conditions (Polaron 3100 apparatus) or used in their wet, hydrogel, form.

2.4. Materials characterization

Scanning electron micrographs of the aerogel foams were obtained using a Hitachi S-4500 apparatus. All the images were taken at a x150 magnification.

The chemical composition of the samples was determined by EDX microprobe on a Cambridge Stereoscan 260 apparatus.

Surface areas were measured by the BET method by nitrogen gas adsorption/desorption at -196°C, using a Micrometrics Tristar apparatus on samples outgassed at 50°C for 5 h. A 50 h outgassing time was also used to verify the effectiveness of the procedure but, as it did not lead to any appreciable improvement, the 5 h time was chosen for the usual procedure.

The thermogravimetric analysis was performed using a Perkin Helmer STA 6000, with a temperature ramp from 35°C to 900°C, at a 2°C/min speed and under air atmosphere.

The Micro-CT scans were obtained by using an X-Ray microtomography instrument Skyscan 1076, with a 18 μm pixel size.

The FTIR spectra were recorded using a Bruker Vector 22 apparatus. The spectra were recorded in ATR mode, directly on the foam without modification.

2.5. Adsorption of Methylene Blue (MB) dye

In the batch system, the adsorbent (10 mg of alginic acid, in the form of foams) and 50 mL of MB aqueous solution, at the desired concentration (from 100 to 600 $mg \cdot L^{-1}$) and native pH (4-4.5), were poured in a 100 mL flask and stirred for the required time at 23°C. After adsorption, the concentration of MB in the solution was determined by means of a UVIKON 943 (Kontron, Italy)

apparatus. The modeling of the experimental isotherm data was performed by means of Excel and Mathematica® softwares. The adsorption capacity ($mg \cdot g^{-1}$) was calculated by:

$$q_t = \frac{V * (C_0 - C_t)}{W}$$

Where C_0 is the initial concentration and C_t is the concentration at a certain time of MB ($mg \cdot L^{-1}$); V is the volume of the solution used (L) and W the amount of adsorbent (g).

The experimental data were obtained with an error bar of ±4.4%. The figures (adsorption isotherms and kinetic models) with error bars can be found in the Supplementary Materials figures S13 to S15.

3. RESULTS AND DISCUSSION

3.1. Preparation and characterization of sodium alginate-based materials

In order to highlight the effect of the alginate structure, two series of samples with different alginate structures, respectively exceeding in guluronic (**AG1**, 63%G) and mannuronic (**AG2** 33%G) units, were prepared. For each series, the foams were obtained by using three different concentrations of sodium alginate, respectively 4, 6 and 8% w/w for the **AG1** and 8, 10 and 12% w/w for the **AG2**. The alginate solutions were frozen using three sets of temperatures: -20, -80°C and liquid nitrogen, and finally freeze-dried at -54°C to remove ice crystals and generate the macroporosity (See Supplementary Material Figure S2).

At a macroscopic level, all the disks show almost the same aspect, being smooth on one side (the face in contact with the Petri dish during freezing) and slightly corrugated on the other side, a difference which became particularly evident when liquid nitrogen was used for the freezing step, probably due to both low temperature and high freezing speed. The samples at higher concentration (10-12% w/w) have an irregular surface, probably because of the higher viscosity (See Supplementary Material, Table S1) of the starting alginate solution. The use of an optical

microscope revealed the presence of small pores on the corrugate side of the disk and of radial fissures on the smooth side (See Supplementary Material, figure S3A and S3B). The section of the foams was characterized by the presence of long and narrow cells, mostly perpendicular to the two faces (Supplementary Material, Figure S3C).

Scanning electron microscopy of the prepared foams shows an internal sponge-like structure (Figure 1), with long macropores of sizes ranging from median values of 12 to 160 μm (See Supplementary Material, Table S1). A careful observation of the obtained images also showed the textural differences between the series of foams, whose morphology appears to be highly dependent whether on the concentration and composition of the sodium alginate solution or on the freezing temperature used.

Generally speaking, samples containing higher amounts of M units (**AG2**) always show a more accessible and regular structure, with higher diameters of pores. Observing the internal section of the two series (i.e. **AG1** and **AG2**) at a given concentration, this is evident for all of the samples and particularly for materials frozen with liquid nitrogen (Figure 1): **AG2** shows a regular system of elongated, parallel pores in contrast with the nonporous, superposed lamellae of the **AG1** sample.

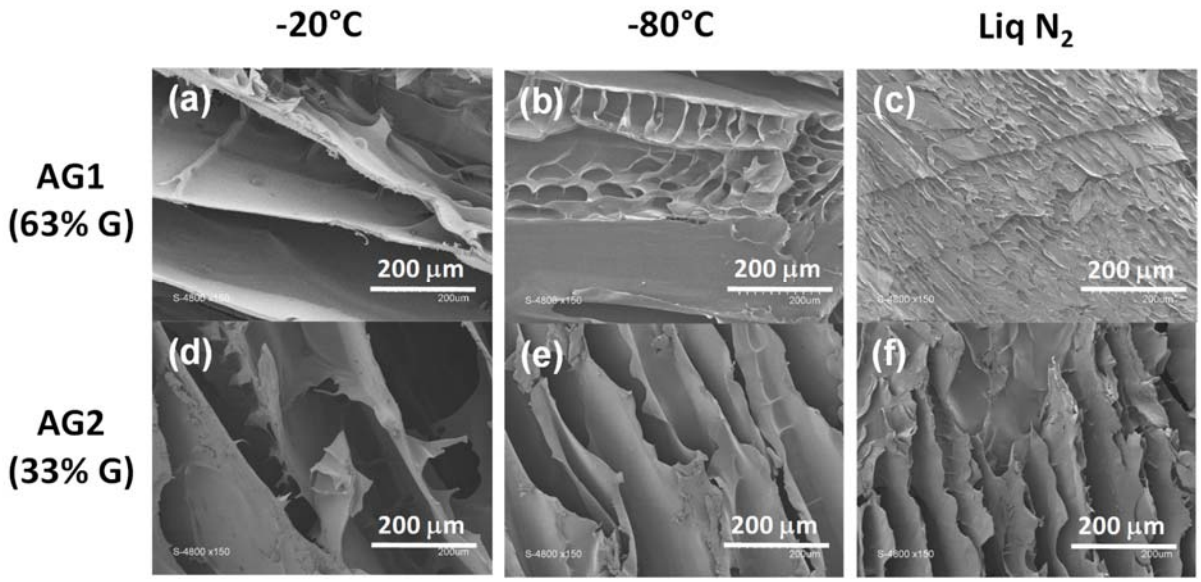

Figure 1. SEM images of the section of foams **AG1** (a, b and c) and **AG2** (d, e and f), 8% w/w, obtained using different temperatures.

The lower accessibility of the **AG1** series is equally evident on the external surfaces, showing in most of the cases a dense structure, sometimes pleated with absent or low porosity (See Supplementary Material, Figure S4). This behavior is in contrast with previous studies on alginate-based meso or macroporous materials reporting an increasing pore diameter with increasing G content (Shapiro, & Cohen, 1997).**Errore. Il segnalibro non è definito.** Since we are reporting the first procedure to sodium alginate foams, instead of divalent cations ionotropic alginate foams, this effect may be ascribed to the absence of a gelation phenomenon. When gelation occurs before freeze-drying, in the presence of divalent ions, the influence of alginate structure, namely G/M ratio, is important in forming the gel framework and in shaping its porosity (Grant, Morris, Rees, Smith, & Thom, 1973). The absence of gelation leads, in the case of **AG1**, to a highly irregular and almost not accessible porosity, particularly evident in samples frozen at -80°C and liquid

nitrogen (see Figure 1b and 1c). The use of lower freezing temperatures, as it will be discussed later, usually leads to the formation of smaller ice crystals (i.e. smaller pores) which, together with the high viscosity of the samples under examination, prevent the formation of proper porous structures. The so frozen **AG1** samples show the presence of closely packed alginate lamellae and no or highly irregular macroporous structures are detected. A slightly different behavior can be noticed at -20°C freezing (Figure 1a), where all the samples show the presence of irregular, interconnected macropores along the whole length of the foam, probably due to the formation of bigger ice crystals. In our process, one of the most important parameters is the viscosity of the starting solutions, which mainly depends on the molecular weight.

On the other hand, all the internal section of **AG2** samples present a regular system of elongated, parallel pores (Figure 1d-f), in contrast with the nonporous, superposed lamellae of the **AG1** samples. Higher amounts of M units (**AG2**) lead to samples with more accessible and regular structure, confirmed by the higher diameter of the pores (See Supplementary Material, Table S1). The absence or irregularity of **AG1** macropores prevented us from obtaining useful information on the effects of concentration and freezing temperature on the porosity and, consequently, **AG2** samples were selected for investigating the effects of concentration and freezing temperatures on the characteristics of final products.

The effect of alginate concentration was assessed by comparing the AG2 foams for a given temperature, namely -80°C (Figure 2). For a given temperature, the initial concentration of sodium alginate only slightly affects the material texture. Samples obtained at 8 and 10% w/w show almost the same morphology, with slightly lower pore diameters in the internal section of the 10% w/w samples. A further increase of the concentration to a 12% w/w value leads in most cases to the decrease of the pore diameters in the internal section, made evident by the replacement of the long

parallel channels, observed for the 8 and 10% w/w concentrations, with smaller and less regular ones (Figure 2d, 2e and 2f). The external surface is also affected by the increased concentration, with the sample at higher concentration being characterized by the presence of few macropores and thicker pore walls (Figure 2a, 2b and 2c).

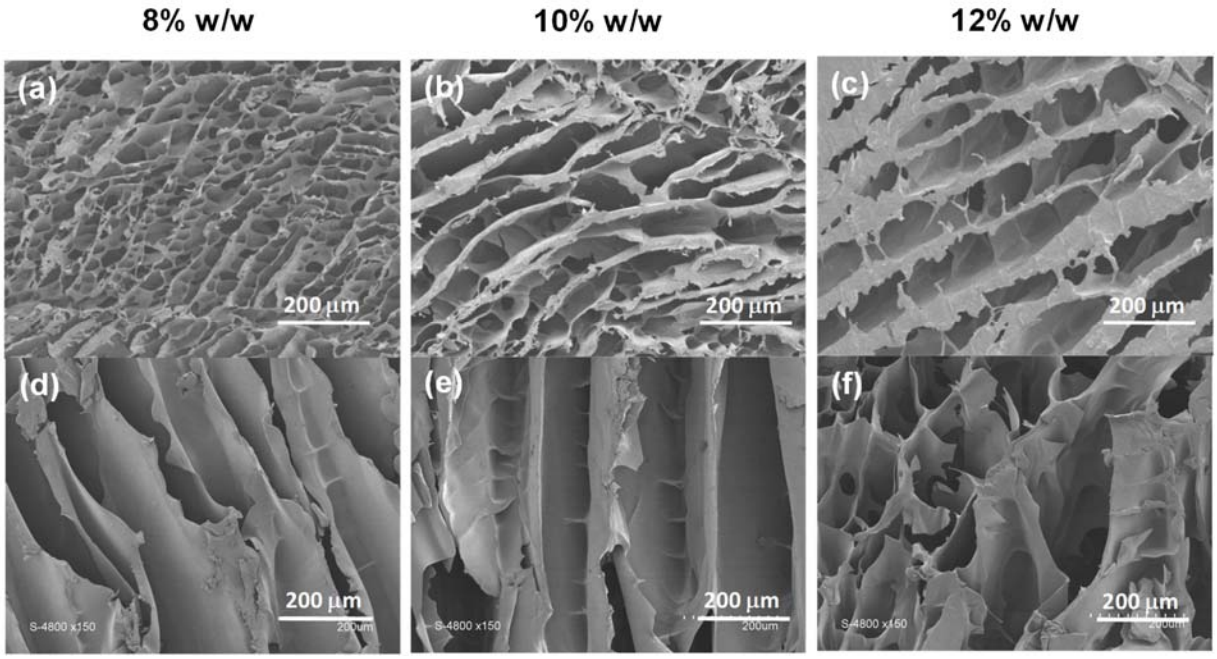

Figure 2. SEM images of the top surface (a, b and c) and cross-sections (d, e and f) of foams AG2, (freezing temperature -80°C) at different alginate concentrations.

Finally, the effect of the freezing temperature on the final texture was examined, confirming that the use of lower temperatures corresponds to progressively smaller and denser pores. All of the **AG2** samples present a regular diminution of the pore diameter, both on the external surface and the internal section, but mantaining a regular and homogeneous texture (Figure 3).

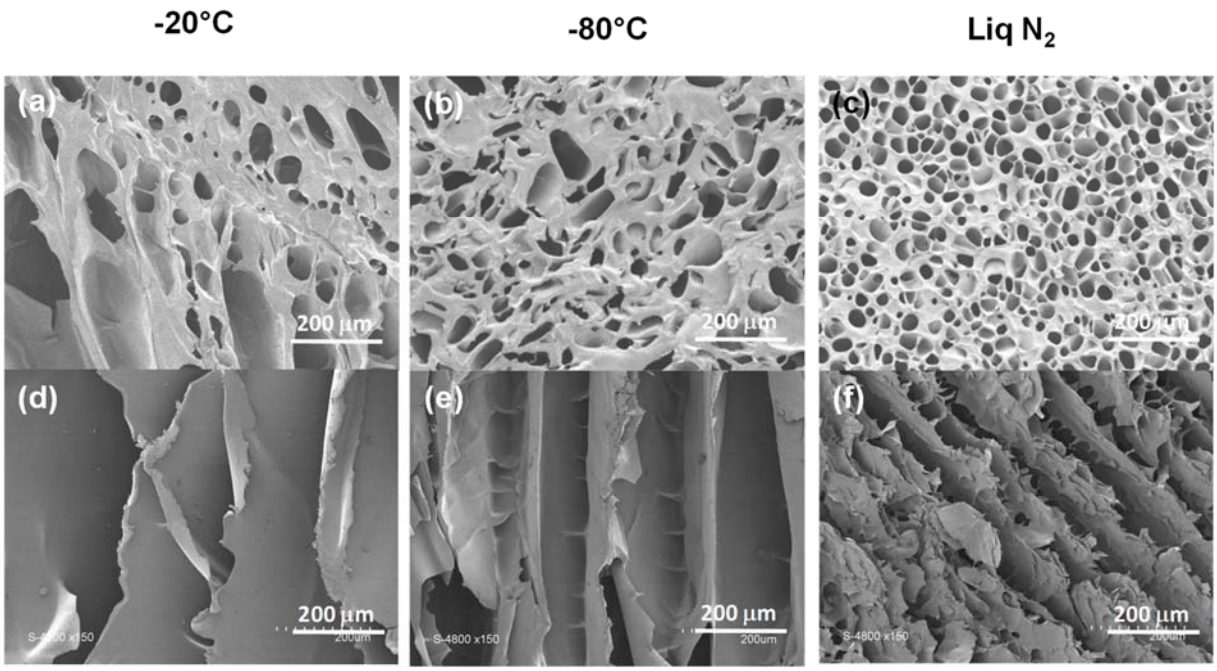

Figure 3. SEM images of the top surface (a, b and c) and cross-sections (d, e and f) surfaces of foams AG2, 10% w/w.

When freezing the alginate solution, the growth of ice crystals is triggered and drives the formation of the foam macropores. The dependency of the pore size on temperature seems to be correlated to different heat transfer rates during the freezing step, with lower freezing rates leading to the formation of larger crystals (i.e. higher temperatures correspond to greater porosities) and fast cooling leading to smaller and more homogeneous crystals (i.e. smaller temperatures correspond to smaller porosities).The size of macropores is highly dependent on the freezing temperature, the lower temperature leading to the smaller macropores. The size of macropores is quite linearly dependent on freezing temperature, except for sample **AG2-12** (12%w/w as the starting concentration. See Supplementary Material, Figure S5). The very high viscosity of the solution is probably the consequence of a change in the organization of macromolecules to a more entangled assembling.

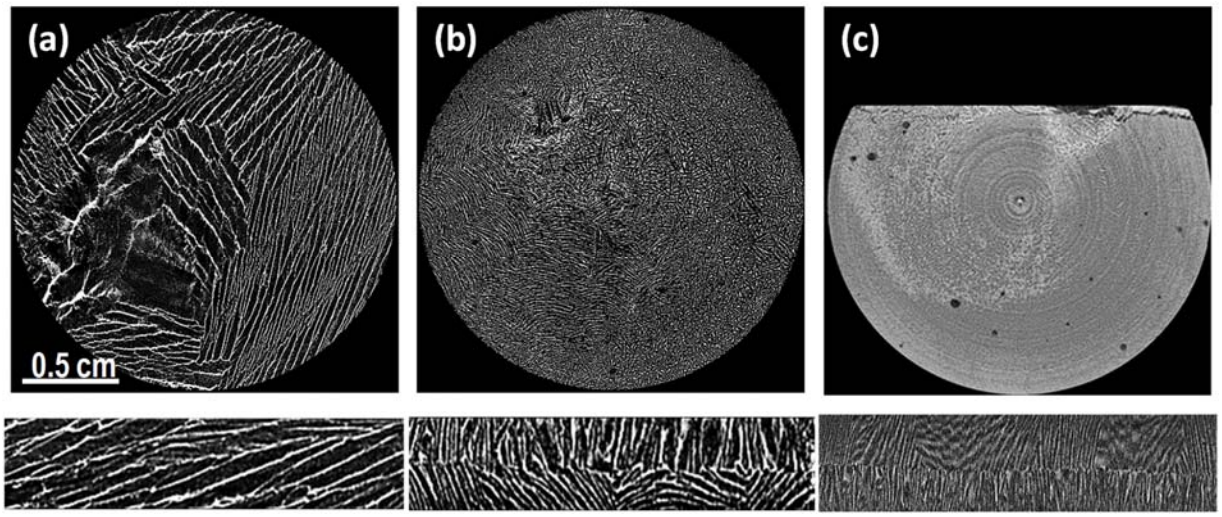

Figure 4. Micro CT images showing the orientation of the pores with the freezing direction transversally (up) and longitudinally (down) for **AG2**, 8% w/w for three freezing temperatures (a) -20°C, (b) -80°C and (c) liq. N_2 temperature.

Microcomputed-Tomography (Micro-CT) of the prepared Na-Alginate foams was performed in order to gain more information on the morphological features of the samples. Using this technique, 2D images of the circular (2 cm diameter, perpendicular to the direction of freezing) and rectangular (2 cm x 0.5 cm, parallel to the direction of freezing) cross-sections of the foams were recorded with a resolution of 18 μm (Figure 4 and Supplementary Material, figures S6 to S8). This analysis allowed fully reconstructing the porosity of the prepared Na-Alginate foams, both longitudinally and transversally to the direction of freezing, giving a strong contribution to the qualitative evaluation of the freezing process. A first information can be obtained on the regularity of the freezing process by observing the evolution of the cross-sections along the direction of freezing. While the samples frozen at -20 °C do not present any significant change in the type of porosity encountered in this direction, the observation of samples frozen at -80 °C and liquid nitrogen shows the presence of two different ice freezing processes. The lower section of the foams (closer to the bottom of the mould) presents a porous structure characterized by the presence of

thin lamellae but, moving to the center, we can notice their progressive replacement by pores of different sizes or orientations. This transition is evident at different extents in all the samples frozen at low temperature and Figure 4 (b and c) shows the central section of foams **AG2**, 8% w/w taken as an example (micro-CT images of **AG1** can be found in the Supplementary Material Figure S7).

This behaviour can be due to the lack of isolation of the upper part of the mould, exposed to the cold atmosphere, resulting in the presence of two contemporary freezing modes: a faster one, coming from the contact between the mould and the cold metal surface, followed by a slower one, due to the formation and growth of ice crystals from above.

Another possible explanation for this two-phase pore structure might be found in the difference in ice nucleation conditions at the solution-glass interface versus secondary nucleation conditions occurring inside the sample, at the solution-ice interface (Madihally, & Matthew, 1999). Micro-CT analysis confirms the trends observed by SEM microscopy, with a generally smaller and less regular porosity for the **AG1** series (see Supplementary Material, Figure S7) and a decrease of the pore sizes with lower freezing temperatures detectable for both systems. The analysis confirms the preferential orientation of the macropores along the direction of freezing even if a certain degree of irregularity is present in almost all the samples.

The results above clearly show that the foam texture (macropore size and distribution) can be easily controlled by varying alginate composition, concentration and freezing temperature. In particular, the porous network was found to depend highly on the viscosity of the starting solution and on the freezing temperature, with increasing viscosities and lower temperatures leading to smaller and less regular porosities. These observations cast a light on the possibility to tailor the morphology of the foams (macropore size and distribution) by applying simple modifications to the preparation procedure. Micro-CT images also showed the presence of a two-phase porous

structure, due to different ice freezing mechanisms. This behavior could, perhaps, be limited by subjecting Na-alginate to a rigorously unidirectional freezing at constant cooling rate, for example by immersing at constant speed the alginate mould in a cooling bath at the desired temperature or modifying the shape and material of the moulds.

A more homogeneous pore structure would of course be preferred, especially for flow applications in catalysis or adsorption. To achieve that, we could try to prevent or limit the formation of ice crystals on the other side of the alginate solution (which is not directly in contact with the cold surface), by, for example, isolating the other side of the mould to force the growth of the ice crystals from only one side. We could also play on the design and the material constituting the mould, in order to control better the thermal transfer properties. A very recent publication on nanofibrillated cellulose aerogels synthesized by freeze-drying nicely evidenced the influence of the mould on the final materials structures (Jimenez-Saelices, Seantier, Cathala, & Grohens, 2017).

As a drawback, all of the prepared sodium alginate foams, present a complete absence of mesoporous structures, as confirmed by a BET surface area of $<2 m^2.g^{-1}$, reported by means of nitrogen adsorption/desorption measurements.

3.2. Preparation and characterization of alginic acid foams

Since sodium alginate foams are water soluble, they are not suitable for remediation applications. To overcome this drawback and obtain a material with a higher surface area and a hierarchical macro-mesoporosity, the sodium alginate foams were acidified by means of the above described procedure. For the acidification step, both water and two CH_3CN/H_2O mixtures (80:20, 50:50) were tested (Supplementary Material, Table S2) and water was finally chosen as a solvent. As an example, three **AG2** samples at a specific concentration (8%w/w) and varying freezing

temperatures were examined to evaluate the effects of this functionalization. The efficient acidification of the samples was confirmed by FT-IR spectroscopy measurements, observing the presence of the signal at 1735 cm^{-1}, typical of the protonated O-C-O group (See Supplementary Material Figure S9) (Sakugawa, Ikeda, Takemura, & Ono, 2004; Valentin et al., 2006).

Under such conditions, the SEM images show the presence of the typical alginic acid fibrous network, coupled with mostly irregular macropores (See Supplementary Material, Figure S10), in all samples.

The use of water as acidification medium led to concomitant acid gelation and unwanted partial dissolution of the water soluble sodium alginate. This phenomenon, in addition to the swelling due to the formation on alginic acid hydrogel, partially destroyed the initial regular macroporosity, especially when foams with smaller porosities (i.e. frozen by means of liquid N_2) were treated.

Nevertheless, samples frozen at higher temperatures, -20°C and -80°C, maintain a satisfying pore size and dispersion, gaining at the same time a surface area comparable with that showed by previously reported alginic acid aerogel formulations (Supplementary Material, Table S3). Based on the above discussion, the alginic acid foams obtained using a 8% w/w sodium alginate solution, enriched in mannuronic units and frozen at -80°C were selected as a model (named **H-F**) for bioremediation applications.

3.3. Efficiency of alginic foams in dye adsorption

The removal of an organic dye from aqueous solutions was tested as a model application, in order to evaluate the adsorption properties of the previously obtained and characterized alginic acid foams. Since the carboxylic functional groups contained in the alginic acid foam may allow the formation of acid-base interactions, we chose a basic dye, methylene blue (3,7-bis(dimethylamino)phenothiazin-5-ium chloride trihydrate, **MB**, (see the structure on

Supplementary Material figure S1) as a first example of application. The results of the adsorption of MB on alginic acid foams are presented through sorption isotherms and uptake kinetics.

3.3.1. Effect of adsorption time and dye concentration

Sorption processes are generally applied for the treatment of dilute effluents. For high-content solutions, the concentration factor expected by coupling sorption and desorption processes is not sufficient for justifying the use of this technique. However, in the present study we extended the range of concentration for achieving the saturation of the sorbent and for evaluating the isotherm characteristics of the system.

In order to determine the equilibrium conditions of the adsorption process, in which the amount of the dye desorbing from the adsorbent is in a state of dynamic equilibrium with the amount of the dye being adsorbed, a series of contact time experiments were performed at different MB concentrations, ranging from 100 to 600 $mg \cdot L^{-1}$. As can be seen from Figure 5, the adsorption (measured by the adsorption capacity at the chosen time, q_t) proceeds rapidly for the first 3 h, probably employing the surface active sites of the materials, and then it slowly approaches the equilibrium point beyond which no more dye is removed from solution under those operating conditions. The initial concentration of the dye has a strong influence on the adsorption process, with an adsorption capacity at equilibrium that increases when increasing the concentration. The equilibrium time is also affected by the initial dye concentration, with lower MB concentrations (100 $mg \cdot L^{-1}$) showing an equilibrium time of about 8 h, while higher concentrations (from 200 to 600$mg \cdot L^{-1}$) require more than 24 h. These data confirm that the selected adsorbent **H-F** is able to adsorb MB in the operating conditions and allow selecting the equilibrium time to 48h to determine the adsorption isotherms.

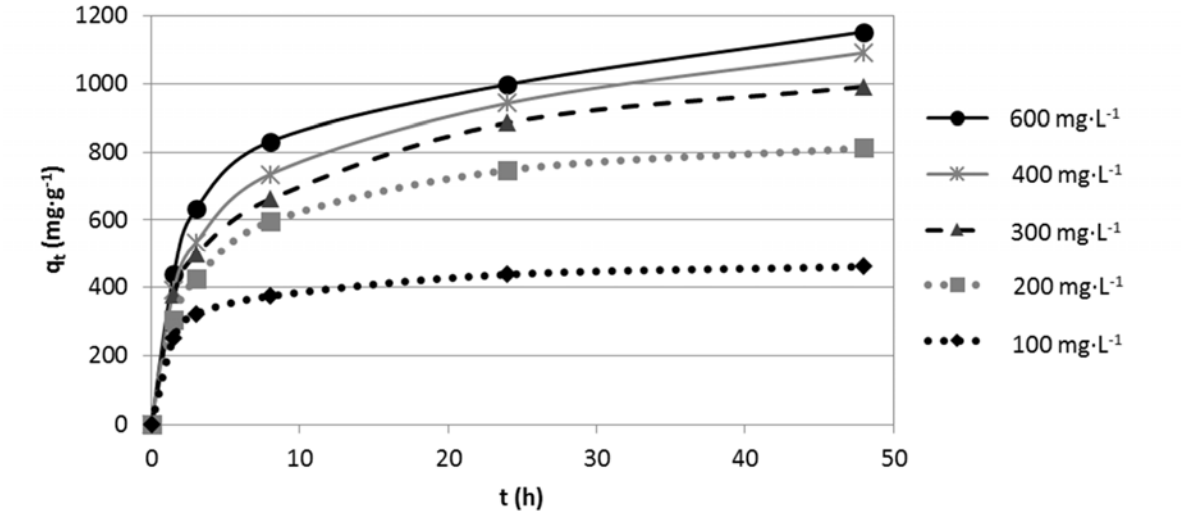

Figure 5. Adsorption capacity (mg·g^{-1}) vs. adsorption time at various initial dye concentrations (in mg·L^{-1})

3.3.2. Adsorption isotherms

Once established the equilibrium time, the adsorption isotherms were derived in order to better understand the nature of the interaction occurring between dye and adsorbent. The adsorption isotherm indicates how the adsorbate molecules distribute between the liquid and solid phase at the equilibrium. In this study, adsorption isotherm analysis was performed by means of two common isotherm models: Langmuir and Freundlich. Langmuir isotherm is a mathematic model that assumes the adsorption of a single adsorbate onto a series of equivalent sites on the surface of the solid with monolayer coverage, while Freundlich isotherm is an empirical model commonly used to describe the adsorption on heterogeneous surfaces with different adsorption sites (Weber, 1972). A 48 h adsorption time was used (Figure 6), in order to ensure the complete equilibrium of the system, and the applicability of the isotherm equation was compared by judging the correlation coefficients, R^2. For both models, linear and non-linear regression analyses were applied to the experimental data, with good agreement (Supplementary Material, Table S4 and S5).

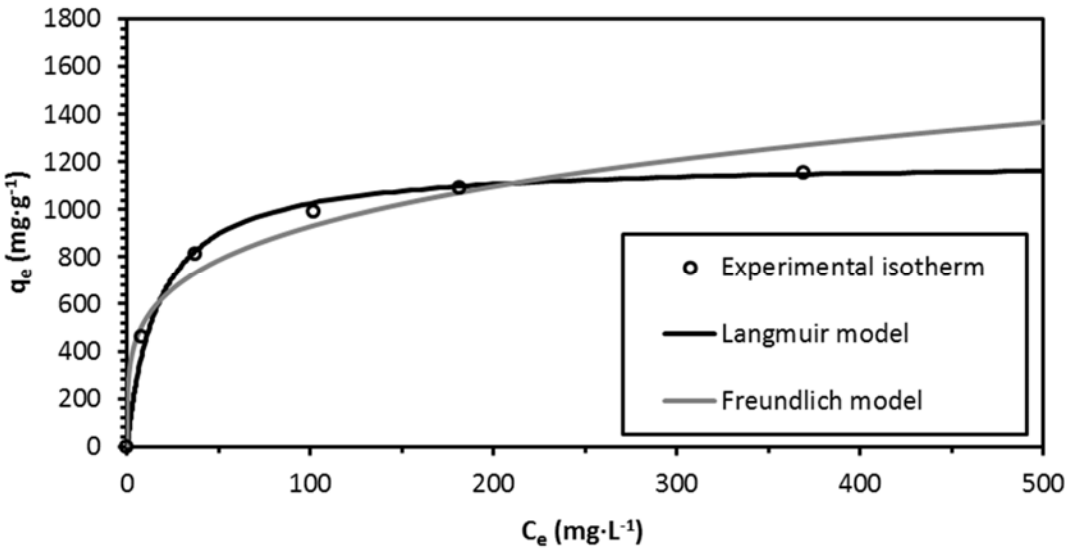

Figure 6. Equilibrium adsorption isotherms of MB on **H-F**, at 24h

The linear form of Langmuir's isotherm model is given by the following equation:

$$\frac{1}{q_e} = \frac{1}{q_m} + \frac{1}{q_m * b * C_e}$$

Where C_e is the equilibrium concentration of the dye (mg·L^{-1}) measured after 48 h, q_e the amount of dye adsorbed per unit mass of adsorbent (mg·g^{-1}) and q_m and b are Langmuir constants related to the maximum adsorption capacity at the saturation of the monolayer and the rate of adsorption, respectively. When $1/q_e$ was plotted against $1/C_e$, a straight line (Supplementary Material, Figure S11) was obtained and the Langmuir constants b and q_m were calculated (Table 1).

Table 1. Langmuir and Freundlich constants

Langmuir isotherm	Freundlich isotherm
qm= 1201 mg·g^{-1}	KF = 308(mg/g)·(L/mg)$^{1/n}$
b = 0.059 L·mg^{-1}	1/n = 0.240
R^2 = 0.999	R^2 = 0.944

The linearized Freundlich isotherm model can be expressed by the following equation:

$$logq_e = logK_F + \frac{1}{n} logC_e$$

Where q_e is the amount of dye adsorbed at the equilibrium per gram of adsorbent ($mg \cdot g^{-1}$), C_e is the equilibrium concentration of the adsorbate and K_F ($(mg/g) \cdot (L/mg)^{1/n}$) and n are Freundlich constants for a given adsorbate and adsorbent at a particular temperature. The slope $1/n$, ranging between 0 and 1, is a measure of adsorption intensity or surface heterogeneity, becoming more heterogeneous as its value gets closer to zero. A value for $1/n$ below 1 indicates a monolayer and non-cooperative adsorption while $1/n$ above 1 is indicative of cooperative adsorption (Hameed, Din, & Ahmad, 2007). The plot of *log* q_e versus *log C* was derived (Supplementary Material, Figure S12) and the results are reported in Table 1.

The experimental data at equilibrium satisfactorily fit the Langmuir model, suggesting a monolayer adsorption. The q_m value, obtained from the Langmuir model, can be used to compare our foam **H-F** with other previously studied adsorbents (Table 2), confirming the good affinity of the developed material for the cationic dye under study. The q_m value corresponds to ca. 3.8 mmol/g of active sites occupied by MB, which represents 70% of monolayer coverage as the starting alginate bears ca. 5.6 mmol/g of carboxylic units. Interestingly, our system demonstrates higher sorption capacity than that obtained with commercial activated carbon and compares well with other biomass-derived adsorbents (Table 2). While the q_m value is still lower than some obtained with organic-inorganic composites found in the literature, as, for example TiO_2 doped sodium alginate crosslinked polyacrylic acid hydrogel which yielded a q_m=2257.36 $mg.g^{-1}$ (Thakur, Pandey, & Arotiba, 2016), the directness of this approach, which employs simple unmodified material, should be recognized.

Table 2. Adsorption of methylene blue on some low-cost biosorbents.

Adsorbent	q_m (mg·g-1)
H-F	1201
Commercial activated carbon (Kannan, & Sundaram, 2001)	980
Straw activated carbon (Weber, 1972)	472
Bamboo based activated carbon (Valentin et al., 2006)	454
Clay (Almeida et al., 2009)	300
Papaya seeds (Hameed, 2009)	556
Teak wood bark (McKay, Porter, & Prasad, 1999)	914
Caulerpa lentillifera (Marungrueng, & Pavasant, 2007)	417
Alga Sargassum muticum seaweed (Rubin et al., 2005)	279
AC on magneticalginate beads (Rocher, Bee, Siaugue, & Cabuil, 2010)	262

3.3.3. Adsorption kinetics

Adsorption kinetics were derived by means of pseudo first (Supplementary Material, Figure S13 and Table S6) and pseudo second order kinetic models, in order to evaluate the adsorption reaction order. The data were also evaluated through the intra-particle diffusion model, i. e. the Morris & Weber equation (Morris, & Weber, 1963) to evaluate the resistance to intra-particle diffusion (Supplementary Material, Figure S16 and Table S8). This model is a simplified approach of resistance to intra-particle diffusion and allows evaluating the existence of several intra-particle diffusion regimes and the existence of several adsorption mechanisms (Thakur, Pandey, & Arotiba, 2016).

The experimental data fit well with the pseudo second-order reaction kinetic mode; its equation is expressed as:

$$\frac{t}{q_t} = \frac{1}{k_2 q_e^2} + \frac{t}{q_e}$$

Where k_2 ($g \cdot mg^{-1} \cdot h^{-1}$) is the rate constant of second-order adsorption. It is noteworthy that the pseudo-second order rate equation was initially developed for the kinetic modeling of homogeneous chemical reactions. Later, this equation was successfully used for describing the kinetic rate of sorption processes (meaning heterogeneous systems). It is thus important to consider that the rate constants are apparent constants that intrinsically integrate the relative contribution of mechanisms of resistance to diffusion (especially intra-particle diffusion).

The linear plot of t/q_t versus t (Supplementary Material, Figure S14) shows good fitting with the experimental q_e data, with calculated adsorption coefficients in accordance with the experimental ones and R^2 values > 0.99 (Supplementary Material, table S7). These results prove the applicability of the pseudo second-order kinetic equation to the adsorption process of MB on the selected alginic acid foam **H-F**. The pseudo second-order rate expression relies on the assumption that the sharing or exchange of electrons between the adsorbent and adsorbate may be the rate-limiting step of the adsorption process.

When looking at the intra-particle diffusion model, for each MB concentration tested, the plots $q_t = f(t^{0.5})$ cannot be represented as a single straight line passing through the origin (Supplementary Material, Figure S16). This result shows that adsorption is clearly not the rate limiting step in our process and probably means that several joint adsorption mechanisms are involved. (Thakur, Pandey, & Arotiba, 2016). We were also able to model all the adsorption curves by two different straight lines, one passing through the origin for lower contact times and another for higher contact times that does not pass through the origin. This result means that different resistance modes, associated to different porosities, are active in the control of uptake kinetics. This is not really

surprising as we synthesized foams exhibiting two populations of pores, macropores and mesopores.

Based on this premise, even if the adsorption in our MB/**H-F** system can be ascribed to a synergic effect of different interaction modes (acid-base interactions between carboxylic and amino groups, electron donor-acceptor interactions with the dye aromatic portion, π-π stacking between the adsorbed molecules, etc), the good fitting of the experimental data with the pseudo second-order kinetics suggests a predominant contribution of the acid-base interaction. In addition, based on the pKa values of mannuronic and guluronic acid (which are in the range of 3.4-3.6), it is possible to suggest that in acidic solutions (at pH below 3.5) carboxylate groups are protonated and poorly available for binding of a cationic dye. The pKa of methylene blue is 3.8. So working at pH close to 4-4.5 reveals consistent with the electrostatic attraction/ion –exchange mechanism of interaction between carboxylate groups of the biopolymer and the cationic groups of the dye, as it has been already evidenced in the work of Thakur et al. on the adsorption of MB on sodium alginate-based organic/inorganic composite hydrogels (Thakur, Pandey, & Arotiba, 2016). Further studies are, of course, needed, to precisely assess the pH effect on adsorption and confirm the exact adsorption mechanism.

4. CONCLUSIONS

This paper reports the preparation and the characterization of the macroporous structures of novel sodium alginate foams obtained by ice-templating coupled with freeze-drying processes. The structure of alginate and the freezing temperature highly affect the textural properties of the foams. Further acidification leads to a macro/meso-porous alginic acid foams. Adsorption of a cationic dye (methylene blue) from aqueous solutions was chosen to evaluate the potential applicability of the foams. A comparison with previously reported adsorbents confirms that the

alginic acid foam under study can be considered a competitive low cost candidate for methylene blue adsorption, considering its good performances related to its wide availability and cheapness. The presence of long and regular channels going through the bulk material coupled with the high potential for functionalization offered by the alginate structure, may improve the potential of the obtained material in flow processes.

AUTHOR INFORMATION

Corresponding Author

*E-mail: nathalie.tanchoux@enscm.fr

ORCID®

Nathalie Tanchoux: 0000-0002-4265-6740

Notes

The authors declare no competing financial interests.

ACKNOWLEDGMENTS

This work was co-funded through a SINCHEM Grant. SINCHEM is a Joint Doctorate programme selected under the Erasmus Mundus Action 1 Programme (FPA 2013-0037). CT-scans showed in this work were produced through the technical facilities of the MRI platform and of the labEx CeMEB

REFERENCES

Agulhon, P., Markova, V., Robitzer, M., Quignard, F., & Mineva, T. (2012). Structure of Alginate Gels: Interaction of Diuronate Units with Divalent Cations from Density Functional Calculations. *Biomacromolecules*, *13*, 1899-1907.

Agulhon, P., Robitzer, M., David, L., & Quignard, F. (2012). Structural Regime Identification in Ionotropic Alginate Gels: influence of the cation nature and alginate structure. *Biomacromolecules*, *13*, 215-220.

Almeida, C. A. P., Debacher, N. A., Downs, A. J., Cottet, L., & Mello, C. A. D. (2009). Removal of Methylene Blue from Colored Effluents by Adsorption on Montmorillonite Clay. *Journal of Colloid and Interface Science*, *332*, 46-53.

An, B., Lee, H., Lee, S., Lee, S. H., & Choi, J. W. (2015). Determining the Selectivity of Divalent Metal Cations for the Carboxyl Group of Alginate Hydrogel Beads during Competitive Sorption. *Journal of Hazardous Materials*, *298*, 11-18.

Chiou, M. S., Ho, P. Y., & Li, H. Y. (2004). Adsorption of Anionic Dyes in Acid Solutions using Chemically Cross-Linked Chitosan Beads. *Dyes and Pigments*, *60*, 69-84.

Crini, G. (2005). Recent Developments in Polysaccharide-Based Materials used as Adsorbents in Wastewater Treatment. *Progress in Polymer Sci*ence, *30*, 38-70.

Dhainaut, J., Deville, S., Amirouche, I., & Klotz, M. (2016). A Reliable Method for the Preparation of Multiporous Alumina Monoliths by Ice-Templating. *Inorganics, 2016, 4*, 6.

Grant, G. T., Morris, E. R., Rees, D. A., Smith, P. J. C., & Thom, D. (1973). Biological Interactions between Polysaccharides and Divalent Cations: the Egg-Box Model. *FEBS Letters, 32*, 195-198.

Guibal, E., Vincent, T., & Jouannin, C (2009). Immobilization of Extractants in Biopolymer Capsules for the Synthesis of New Resins: a Focus on the Encapsulation of Tetraalkyl Phosphonium Ionic Liquids. *Journal of Materials Chemistry*, *19*, 8515-8527.

Hadinoto, K., & Yang, Y. (2014). Continuous and Sustainable Granulation of Nanopharmaceuticals by Spray Coagulation Encapsulation in Alginate. *International Journal of Pharmaceutics*, *473*, 644-652.

Hameed, B.H. (2009). Evaluation of Papaya Seeds as a Novel Non-Conventional Low-Cost Adsorbent for Removal of Methylene Blue. *Journal of Hazardous Materials*, *162*, 939–944.

Hameed, B. H., Din A. T. M., & Ahmad, A. L. (2007). Adsorption of Methylene Blue onto Bamboo-Based Activated Carbon: Kinetics and Equilibrium Studies. *Journal of Hazardous Materials*, *141*, 819-825.

Jimenez-Saelices, C., Seantier, B., Cathala, B., & Grohens, Y. (2017). Effect of freeze-drying parameters on the microstructure and thermal insulating properties of nanofibrillated cellulose aerogels. *Journal of Sol-Gel Science and Technology*, 1-11.

Jouannin, C., Dez, I., Gaumont, A. C., Taulemesse, J. M., Vincent, T., & Guibal, E. (2011). Palladium Supported on Alginate/Ionic Liquid Highly Porous Monoliths: Application to 4-nitroaniline Hydrogenation. *Applied Catalysis B: Environmental*, *103*, 444-452.

Jung, W., Jeon, B. H., Cho, D. W., Roh, H. S., Cho, Y., Kim, S. J., & Lee, D. S. (2015). Sorptive Removal of Heavy Metals with Nano-sized Carbon Immobilized Alginate Beads. *Journal of Industrial and Engineering Chemistry*, *26*, 364–369.

Kannan, N., & Sundaram, M.M. (2001). Kinetics and Mechanism of Removal of Methylene Blue by Adsorption on Various Carbons—a Comparative Study. *Dyes Pigments*, *51*, 25-40.

Ki, S. B., Singh, D., Kim, S. C., Son, T. W., & Han, S. S. (2013). Effect of cross-linkers in fabrication of carrageenan–alginate matrices for tissue engineering application. *Biotechnology and Applied Biochemistry, 60*, 589-595.

Klotz, M., Amirouche, I., Guizard, C., Viazzi, C., & Deville, S. (2012). Ice Templating—An Alternative Technology to Produce Micromonoliths *Advanced Engineering Materials*, *14*, 1123–1127.

Krys, P., Testa, F., Trochimczuk, A., Pin, C., Taulemesse, J. M., Vincent, T., & Guibal, E. (2013). Encapsulation of Ammonium Molybdophosphate and Zirconium Phosphate in Alginate Matrix for the Sorption of Rubidium (I). *Journal of Colloid and Interface Science*, *409*, 141-150.

McKay, G., Porter, J.F., & Prasad, G.R. (1999). The Removal of Dye Colours from Aqueous Solutions by Adsorption on Low-Cost Materials. *Water, Air, & Soil Pollution*, *114*, 423–438.

Madihally, S. V., & Matthew, H. W. T. (1999). Porous Chitosan Scaffolds for Tissue Engineering. *Biomaterials*, *20*, 1133-1142.

Martinsen, A., Skjakbraek, G., Smidsrod, O., Zanetti, F., & Paoletti, S. (1991). Comparison of different methods for determination of molecular-weight and molecular-weight distribution of alginates. *Carbohydrate Polymers*, *15*, 171–193.

Marungrueng, K., & Pavasant, P. (2007). High Performance Biosorbent (Caulerpa lentillifera) for Basic Dye Removal. *Bioresource Technology*, *98*, 1567–1572.

Weber, W. J., & Morris, J. C. (1963). Kinetics of adsorption on carbon from solution. *Journal of the Sanitary Engineering Division*, *89*, 31-60.

Pandey, S. (2017). A comprehensive review on recent developments in bentonite-based materials used as adsorbents for wastewater treatment. *Journal of Molecular Liquids, 241*, 1091-1113.

Pandey, S., Ramontja, J. (2016). Turning to Nanotechnology for Water Pollution Control: Applications of Nanocomposites. *Focus on Science, 2*, 1-10.

Pettignano A. (2016). Alginate: a Versatile biopolymer for functional advanced materials. PhD thesis, Montpellier, France.

Raei, M., Rajabzadeh, G., Zibaei, S., Jafari, S. M., & Sani, A. M. (2015). Nano-encapsulation of Isolated Lactoferrin from Camel Milk by Calcium Alginate and Evaluation of its Release. *International Journal of Biological Macromolecules*, *79*, 669-673.

Rafatullaha, M., Sulaimana, O., Hashima, R., & Ahmadb, A. (2010). Adsorption of Methylene Blue on Low-Cost Adsorbents: a review. *Journal of Hazardous Materials*, *177*, 70-80.

Rocher, V., Bee, A., Siaugue, J. M., & Cabuil, V. (2010). Dye Removal from Aqueous Solution by Magnetic Alginate Beads Crosslinked with Epichlorohydrin. *Journal of Hazardous Materials*, *178*, 434-439.

Rubin, E., Rodriguez, P., Herrero, R., Cremades, J., Barbara, I., & Sastre de Vicente, M.E. (2005). Removal of Methylene Blue from Aqueous Solutions using as Biosorbent Sargassum

Muticum: an Invasive Macroalga in Europe. *Journal of Chemical Technology and Biotechnology*, *80*, 291–298.

Sakugawa, K., Ikeda, A., Takemura, A., & Ono, H. (2004). Simplified Method for Estimation of Composition of Alginates by FTIR. *Journal of Applied Polymer Science***,** 93, 1372-1377.

Sarker, B., Rompf, J., Silva, R., Lang, N., Detsch, R., Kaschta, J., Fabry, B., & Boccaccini, A. (2015). R. Alginate-based Hydrogels with Improved Adhesive Properties for Cell Encapsulation. *International Journal of Biological Macromolecules*, *78*, 72-78.

Shapiro, L., & Cohen, S. (1997). Novel Alginate Sponges for Cell Culture and Transplantation. *Biomaterials*, *18*, 583-590.

Thakur, S., Pandey, S., & Arotiba, O. A. (2016). Development of a sodium alginate-based organic/inorganic superabsorbent composite hydrogel for adsorption of methylene blue. *Carbohydrate Polymers*, *153*, 34–46.

Valentin, R., Horga, R., Bonelli, B., Garrone, E., Di Renzo, F., & Quignard F. (2006). FTIR Spectroscopy of NH3 on Acidic and Ionotropic Alginate Aerogels. *Biomacromolecules*, *7*, 877-882.

Vincent, C., Barre, Y., Vincent, T., Taulemesse, J. M., Robitzer, M., & Guibal, E. (2015). Chitin-Prussian Blue Sponges for Cs (I) Recovery: From Synthesis to Application in the Treatment of Accidental Dumping of Metal-Bearing Solutions. *Journal of Hazardous Materials*, *287*, 171-179.

Weber W. J. (1972). *Physico-chemical Processes for Water Quality Control*; Wiley Interscience: New York.

Zmora, S., Glicklis, R., & Cohen, S. (2002). Tailoring the Pore Architecture in 3-D alginate Scaffolds by Controlling the Freezing Regime during Fabrication. *Biomaterials*, *23*, 4087–4094.